A Parametric, Optimization-based Study on the Feasibility of a Multi-Segment Antisolvent Crystallizer for In-Situ Fines Removal and Matching of Target Size Distribution

Bradley J. Ridder[1], Aniruddha Majumder,[2,3] and Zoltan K. Nagy[1,2*]

[1]School of Chemical Engineering, Purdue University, West Lafayette, Indiana, USA

[2]Department of Chemical Engineering, Loughborough University, Loughborough, LE11 3TU, UK

[3]School of Engineering, University of Aberdeen, Aberdeen, AB24 3UE, UK

*Corresponding author: Email: zknagy@purdue.edu; Phone: +1 765 494 0734; Fax: +1 765 494 0805.

ABSTRACT

We have computationally investigated the use of the multi-segment, multi-addition, plug-flow crystallizer (MSMA-PFC) for use in producing pharmaceutical crystals. A population balance framework was used to model the crystallization process. The dissolution of crystals can be modeled when solubility is below saturation. The evolved volume fraction distributions were optimized in a least-squares sense by manipulating a vector of decision variables in order to hit a target volume fraction distribution. The genetic algorithm was used for optimization. A reduced orthogonal array experimental design was used to examine the effect of several kinetic parameters and total crystallizer length. The results indicate that the parameters which govern nucleation are the most sensitive, followed by those for growth. Dissolution does not appreciably occur in any of the optimizations. The reason the optimization does not add any pure solvent is

likely due to the addition of pure solvent causing a simultaneous decrease in concentration and decrease in residence time, which the optimization judges to be sub-optimal.

Keywords: Antisolvent crystallization, Population balance, Crystallization optimization

1. Introduction

1.1 Continuous crystallization

Continuous crystallization of pharmaceuticals has attracted much interest in recent years as a cheaper, more efficient alternative to batch-wise purification.[1–5] This is part of an overall much broader research effort aimed at developing fully continuous pharmaceutical manufacturing systems, including reactors, crystallizers, granulators, and tableting machines – among others.[6–9] Crystallization is of special interest due to its ubiquity in pharmaceuticals – over 80% of active pharmaceutical ingredients (API) are purified by crystallization.[10] The process is widely used in the agrochemical and fine chemicals industries as well. [11,12]

1.2 Motivation for In-Situ Removal of Fine Crystals

While purification is the main motive behind crystallization, the crystal size distribution (CSD) affects downstream operations and the ameliorative properties of the final dosage form. The curative properties of the final dosage form are dependent on the dissolution rate and bioavailability, which are strongly affected by the CSD and other particle properties.[13,14] Downstream processes affected by CSD shape include filtering, washing, and drying.[15] The presence of fine crystals greatly encumbers these operations.

The typical method of removing fines is to classify the product crystals, re-dissolve the fines, separate the antisolvent when feasible, and recycle the mixture back to the crystallization system. However, this method is problematic. Classification, recycle, and stream separation require further process equipment, increasing capital and operating costs. Classification combined with recycle has been mathematically deduced (and subsequently observed) to impart oscillatory dynamics to the CSD[12]. These oscillations make it difficult to obtain a consistent product. Furthermore, from a risk analysis viewpoint, extra equipment is generally "more things that can go wrong", and presents another route by which microbes could contaminate the manufacturing process. It would be good if we could eliminate fines altogether by an in-situ approach.

1.3   Prior Work on In-Situ Fines Removal

Previous work by Abu Bakar et al. and Majumder and Nagy explored the concept of "in-situ" fines removal, where the operation of the crystallizer actively eliminates fine crystals during the crystallization by means of dissolution.[13,16] With this approach, classification, re-dissolving, and stream separation are rendered (in theory) unnecessary. The work by Majumder and Nagy most closely follows our work here. [16] In that work, a constrained nonlinear optimization problem was solved to identify temperature profiles that would match a target distribution in a least-squares sense by removing fine crystals.

1.3.1   Cooling Crystallization versus Antisolvent Crystallization: The Coupling of Antisolvent Addition with Concentration and with Residence Time

Majumder and Nagy previously investigated computationally the use of a multi-segment cooling crystallizer for in-situ fines dissolution.[16] In that work, the decision variables were the jacket temperatures in each segment, which allowed the particular segment to go above or below solubility as necessary to dissolve the fine crystals and grow large ones. Ridder et al. have

modeled and optimized a multi-segment antisolvent crystallizer for drug crystal production, but that work did not allow for dissolution to occur. [17,18] This work is an extension of the previous works by Ridder et. al. and Majumder and Nagy, as we are now using an antisolvent crystallization with the capability to dissolve crystals when below solubility.[16] Figure 1 below depicts the path of information flow for a cooling PFC crystallization process, and an antisolvent PFC crystallization process. For an antisolvent crystallization, the decision variables are the flowrates of antisolvent into each segment. As can be seen in the figure, there is no coupling between concentration and residence time in the cooling crystallization. Residence time furthermore, is always constant.

In the antisolvent case however, the addition of solvent reduces the current concentration via dilution. Also, residence time decreases monotonically with each successive segment. As we shall see further ahead, this coupling dramatically increases the difficulty of optimization and the performance of the crystallizer.

(a)   (b)
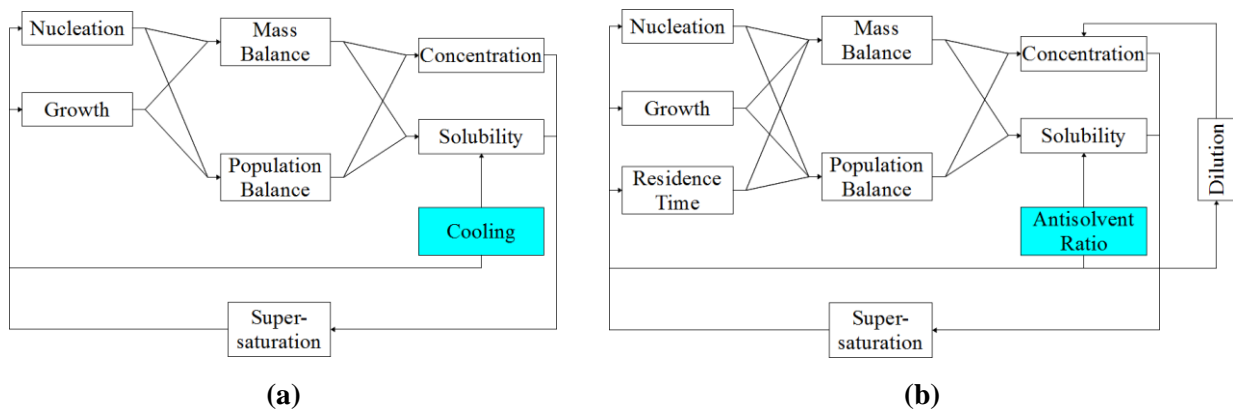
Figure 1. Information flow diagrams in a multisegment crystallizer for (a) cooling crystallization and (b) antisolvent crystallization. The cooling crystallization has no coupling between residence time and the control (jacket temperature), and residence time is constant within each segment. None of this is true in antisolvent

crystallization, since the addition of antisolvent simultaneously affects the current concentration via dilution, and reduces the current residence time due to a mass balance argument.

1.4 Parametric Study via Optimization of the Antisolvent Crystallizer

In this work, we present results for the steady-state operation of a multi-segment, multi-addition, plug-flow crystallizer MSMA-PFC which utilizes dissolution to eliminate fine crystals. We have explored the geometric design parameters of the crystallizer, as well as the kinetic parameters of crystallization. To reiterate, this work is an extension of that by Majumder and Nagy, but for the case of antisolvent crystallization as opposed to a cooling crystallization.[16]

2. Multiple segment, multiple-addition antisolvent plug flow crystallizer (MSMA-PFC) Model Framework

2.1 Model Diagram
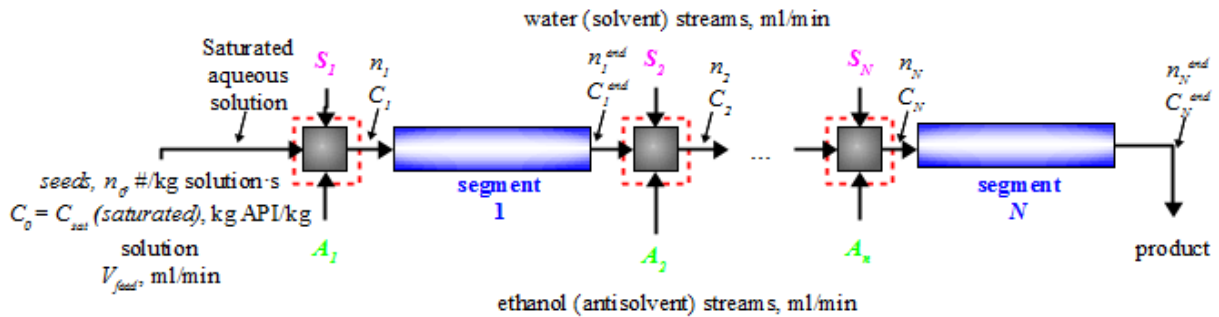
Figure 2. Diagram of the multi-segment, multiple-addition plug flow crystallizer (MSMA-PFC). Seeded liquid solvent, with solute concentration C_0 flows in from the left into a mixing chamber (gray box). The dilution correction factor, γ_j, is applied to the exit stream around each mixing point (red dashed boxes). The combined streams then flow into a plug-flow segment (blue rectangle). Antisolvent reduces solubility, triggering nucleation and growth. Streams of pure solvent are utilized to push the solution below solubility when necessary.

The MSMA-PFC is based on the setup in Alvarez and Myerson.[2] It is modeled as a series of ideal plug flow elements, of equal length, and antisolvent is added at the beginning of each

segment (Figure 2 above). Each of the N segments is a separate PFC, running in steady-state, isothermal operation. The inlet stream (at the far left) feeds saturated mother liquor at flowrate V_{feed} (ml/min), with an initial concentration of solute, C_0 (kg API/kg solution), and a seed CSD, n_0 (# of crystals/kg of solution·m). At each mixing point (gray boxes in the figure) antisolvent flowing at flowrate A_j (ml/min) and pure solvent at flowrate S_j (ml/min), mixes together with the main stream for $j = 1,2, \dots, N$. It is to be noted that we are using mass-intensive units for our state variables, n (# of crystals/kg of solution·m) and C (kg API/kg solution).

2.2 Summation Indices and Segment Indices

Summation indices always use the letter i as a dummy index. The letter j always refers to "for the jth PFC segment." When an index refers to a mixing point, j always refers to the mixing point immediately preceeding the jth PFC segment (e.g. the $j = 1$ mixing point is the very first mixing point on the left hand side in Figure 2 above).

2.3 Effect of Dilution

The addition of streams A_j and S_j to the process causes a decrease in C and n in the oncoming feed stream due to the effect of dilution. Concentration and number density are reduced because the solute mass (and crystal mass) has remained the same, but total volume has increased. There is a double meaning of this term in the literature, as some authors refer to antisolvent crystallization as "dilution."[12] We reiterate that in this paper, we refer to dilution as being the reduction in solute concentration due to the addition of a solute-free liquid at a constant solute mass. To account for this effect, the number density of the jth outgoing stream, n_j (# of crystals/kg of solution·m) about the jth mixing point is multiplied by:

$$\gamma_j = \frac{\rho_j^{solution} V_j^{solution}}{\rho_{j+1}^{solution} V_{j+1}^{solution}} \tag{1}$$

Where $\rho_j^{solution}$ is the density of the solution, and V_j is the volumetric flow rate of the entire stream. $V_j^{solution}$ can be determined by dividing the total solution mass flow rate by the total solution density:

$$V_{j+1}^{solution} = \frac{\rho_{H_2O}\left(V_{feed} + \sum_{i=1}^{j} S_i\right) + \rho_{EtOH} \sum_{i=1}^{j} A_i}{\rho_{j+1}^{solution}} \tag{2}$$

Where ρ_{H_2O} and ρ_{EtOH} are the densities of water as solvent and ethanol as antisolvent (997 kg/m^3 and 785.22 kg/m^3, respectively). The total solution density, $\rho_{j+1}^{solution}$ (kg/m^3), is calculated numerically from a curve fit of the density of an ethanol-water mixture in terms of ethanol mass fraction. These expressions are derived by performing progressively wider mass balances about the mixing points and PFC segments. The method is more easily explained with a diagram (Figure 3 below). The colored boxes demonstrate the pattern one follows to ultimately derive (1) and (2).
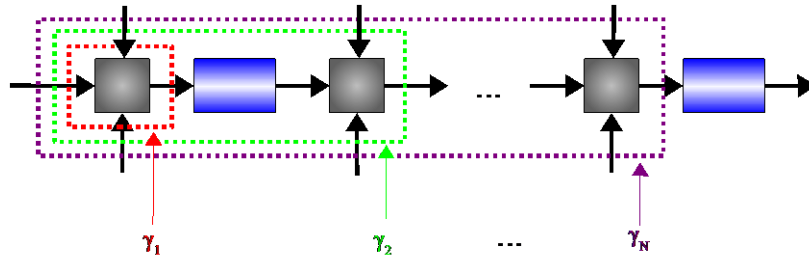
Figure 3. Mass balance envelopes that are used to derive γ dilution correction factor. Incoming streams are positive; outgoing are negative.

After mixing with the solvent and antisolvent streams, the mixture then flows into the jth PFC segment, where nucleation and growth occur. We assume the streams mix on a time scale well below the induction time, and also attain plug-flow. At the exit of the segment, a new size distribution, $n(L, x_j^{end})$, and a

reduced solute concentration, $C(x_j^{end})$, are obtained. We will abbreviate these quantities as n_j^{end} and C_j^{end}. We clarify to the reader that this is not the same as C_{j+1} or n_{j+1}; these quantities are created when the next solvent and antisolvent streams are added; the pattern of indexing is made clear in Figure 2 above. This process continues recursively until the product stream leaves the final, N^{th} segment (product stream). The final crystal size distribution, n_N^{end}, is used for solving the least-squares optimization problem. Both n_N^{end} and C_N^{end} are used to calculate several constraints.

3. Crystal Population and Solute Mass Balance Equations

Simulation of isothermal antisolvent crystallization processes requires two governing equations to be solved simultaneously: the population balance equation, and the mass balance equation.

3.1 Population Balance Equation

Population balances are a mathematical framework for tracking the properties of large populations of entities. Such balances are routinely used in the modeling of crystallization processes for the purpose of tracking size (though other properties, such as composition and shape, can also be plausibly tracked in this way).The first is the population balance equation for solving for the crystal size distribution:

$$u_{x,j}\frac{\partial n_j}{\partial x} + G_j\frac{\partial n_j}{\partial L} = B_{0,j}\delta(L - L_0) \tag{3}$$

Where u_x is the average velocity in the x-direction of the fluid (m/s), n is the crystal size distribution (#/kg of solution·m), x (m) is the length along the crystallizer, G (μm/s or m/s) is the linear crystal growth rate, L (m or μm) is the characteristic crystal length, B_0 is the nucleation rate (# of nucleated crystals/kg solution·s), and $\delta(L - L_0)$ (m⁻¹) is the Dirac delta function, which mathematically describes the assumption that nucleated crystals come into existence with size L_0. L is referred to as the "internal coordinate" since it deals with the properties of entities *within*

the control volume, while x is the "external coordinate", since it is a location in physical space within the control volume. We have assumed simple one-dimensional flow in our pipe, hence why there is only one external coordinate. We believe the assumption of 1-D flow to be valid, given that the Reynolds number for the flows studies was typically in excess of 9000. The j subscript always refers to the value of a quantity in the jth PFC segment.

The average velocity in the x-direction in the jth segment is computed by dividing volumetric flow rate by the cross-sectional tube area:

$$u_{x,j} = \frac{V_j^{solution}}{\pi d_{inner}^2/4} \tag{4}$$

Where d_{inner} is the inner diameter of the crystallizer tube, which is the same for all segments.

3.2 Definition of Moment

The kth-moment of the crystal size distribution in the jth PFC segment is defined by:

$$\mu_{k,j} = \int_0^\infty n_j L^k dL \tag{5}$$

With units of (m^k/kg solution). The interpretation of the first several moments (per kg solution) are:

- μ_0: The total number of crystals.

- μ_1: Measure of the total end-to-end-length of the crystals.

- μ_2: Measure of the total interfacial surface area of the crystals exposed to the solution.

- μ_3: Measure of the total volume of the crystals.

3.3 Mass Balance Equation

The other equation is the mass balance for dissolved drug:

$$\frac{dC_j}{dx} = -\frac{\rho_c k_v}{u_{x,j}}(3G\mu_{2,j} + B_{0,j}L_0^3) \tag{6}$$

The term μ_2 is the second moment of the crystal size distribution (m^2 of crystals/kg solution). C

is the solute concentration in the liquid phase (kg API/kg solution), ρ_c is the density of

crystalline API (assumed to be 1490 kg/m^3), L_0 is the minimum detectable crystal size (m), B_0 is

the nucleation rate (# of nucleated crystals/kg solution·s), and k_v is the dimensionless crystal shape

factor ($\pi/6$ for spheres) [19]. In a pure mathematical treatment, L_0 would simply be set to zero; however,

all instrumentation used in practice for experimentation and process control will have limits to

observability. Equation (6) is an integro-differential equation, since μ_2 is defined by the integral

expression (5).

3.4   Boundary Conditions

For the first segment ($j = 1$), the boundary conditions for these equations are:

$$n_1(L, x = 0) = \gamma_1 n_0$$

$$n_1(L = 0, x) = B_{0,1}/G_1 \tag{7}$$

$$C_1(x = 0) = \gamma_1 C_0$$

Where n_0 is the crystal size distribution of the seed crystals, B_0 is the nucleation rate (#/kg of

solution·s), and C_0 is the initial solute concentration. In subsequent segments ($j \geq 2$), the

boundary conditions become:

$$n_j(L, x = 0) = \gamma_j n_{j-1}^{end}$$

$$n_j(L = 0, x) = B_{0,j}/G_j \tag{8}$$

$$C_j(x = 0) = \gamma_j C_{j-1}^{end}$$

A Gaussian bell curve was used for n_0 (#/kg of solution·m) in all cases, with mean δ_{seed} (m) and

standard deviation ω_{seed} (m):

$$n_0(L) = \frac{N_{total}}{\omega_{seed}\sqrt{2\pi}} \exp\left(-\frac{(L - \delta_{seed})^2}{2\omega_{seed}^2}\right) \tag{9}$$

Where N_{total} is the total number density (# of crystals/kg solution). N_{total} can be interpreted in

(9) as a constant that forces the seed distribution to agree with the specified seed mass loading, λ

(%, dimensionless). The mass balance on the seed distribution is closed by solving the algebraic

equation for N_{total} such that:

$$\lambda C_0 - \rho_c k_v \mu_{3,0} = 0 \tag{10}$$

where $\mu_{3,0}$ is the third moment of the seed distribution. Equation (10) is closed by manipulating

N_{total}, which is embedded in the integral term $\mu_{3,0}$:

$$\mu_{3,0} = \int_0^\infty n_0 L^3 dL \tag{11}$$

3.5   Growth, Nucleation, and Dissolution Rate Laws

The growth and nucleation laws are given by the equations (again, all j subscripts refer to the jth

segment):

$$G_j(S_j) = k_g \sigma_j^g, B_{0,j}(\sigma_j) = k_b \mu_2 \sigma_j^b, D_j(\sigma_j) = -\varphi k_g (1 - \sigma_j)^d$$

$$\sigma_j = C_j(x)/C_{sat,j} \tag{12}$$

where σ is the supersaturation ratio, k_g is the growth rate constant (m/s), g is the growth rate

order, k_b is the nucleation rate constant, b is the nucleation order, D is the dissolution rate (m/s),

d is the dissolution order, and C_{sat} is the solubility concentration (kg API/kg solution). G is

replaced by D in (3) for $\sigma < 1$.

We use a modified version of the growth law for the dissolution rate law. The dissolution rate can be approximated by multiplying the modified version of the growth law by a constant $\varphi > 1$, which adjusts for the fact that dissolution is typically much faster than growth. The calculation of C_{sat} is discussed in section 3.6 below. The values of the kinetic parameters are taken from experimental work by Luo et al. and are included in Table 1.[19] These parameters were chosen because they are expressed in terms of water mass fraction, which is significantly easier to work with than other representations.

Table 1. Physical and chemical property data table used for modeling the antisolvent crystallization.

Parameter	Value
Initial concentration, C_0 [kg API/kg solution]	0.030935
Shape factor k_v, [-]	$\pi/6$
Solid API density ρ_c, [kg/m³]	1490
Dissolution acceleration, φ [-]	250
Number of segments, N [-]	50
Seed crystal mean size, δ_{seed} [μm]	50
Seed crystal standard deviation, ω_{seed} [μm]	10

3.6 Calculation of API Solubility

The solubility of the API in a water-ethanol (solvent-antisolvent) mixture at 25 °C was taken from the experimental data plot provided in Figure 2 of Luo et al. [19] for the case of the drug biapenem. Data points were extracted from the curve, and are given in

Table 2 below. Comparison with various curve fitting methods in MATLAB showed that linear interpolation provided the best fit. The data correspond to a minimum solubility in ethanol as 2.464 mg/ml, and a maximum solubility in water as 30.935 mg/ml.

Table 2. Solubility data for biapenem-water-ethanol system at 25 ℃.

Water Mass Fraction, X_w	C_{sat} x 10^3 (kg solute/kg solution)
0.199	2.464
0.299	2.831
0.398	3.497
0.500	4.463
0.599	6.103
0.699	9.615
0.799	15.299
0.898	21.956
1.000	30.935

The water mass fraction in the jth PFC is computed by:

$$X_{H_2O}^j = \frac{\rho_{H_2O}V_{feed} + \rho_{H_2O}\sum_{i=1}^{j}S_i}{\rho_{H_2O}V_{feed} + \rho_{H_2O}\sum_{i=1}^{j}S_i + \rho_{EtOH}\sum_{i=1}^{j}A_i} \tag{13}$$

Plugging $X_{H_2O}^j$ into the curve fit object created in MATLAB yields the solubility concentration of biapenem, $C_{sat,j}$.

3.7 Solution of Model Equations

A typical method used for solving equations (3) and (6) is to apply the method of moments (MOM), which reduces system to a small number of coupled ordinary differential equations for the moments of the crystal size distribution. However, this method is useless here, since we need the full CSD to be able to match the target distribution. Previous researchers have attempted various deconvolution/inversion methods in the moments to re-construct the crystal size

distribution, but these methods tend to yield poor results and be more trouble than they are worth.[20] A variety of methods have been developed for direct solution of the population balance equation. To solve this system, we have utilized a high-resolution finite volume (FV) technique, which is the combination of the semi-discrete FV technique with the van Leer flux limiter.[16,21] This method provides $O(h^2)$ accuracy where the solution is smooth, without the oscillations found in other methods. Details on the finite volume method are given in Majumder and Nagy.[16]

Equation (3) was discretized into K ordinary differential equations, where K is the number of crystal size bins. The discretization started at 1 μm, and marched upward up to the maximum bin size of 500 μm, for a total of $K = 101$ bins. Equations (3) and (6) are solved simultaneously, with the sixth-order accurate Boole's Rule used to approximate μ_2 in (6). The method marches forward into external space, using 10 steps in external space.

4. Optimization Problem Formulation

Our goal is to eliminate the production of fine crystals by utilizing dissolution. The quality of the elimination is ascertained by measuring how closely the attained volume fraction distribution leaving the Nth PFC ($f_{v,N,end}$) matches a theoretically-best growth-only volume fraction distribution, $f_{v,target}$. The target distribution is generated by simulating the crystallization with only one segment, with nucleation arbitrarily set to zero. With no nucleation, all solute depletion is solely due to crystal growth on the seeds, and no fine crystals are ever created. Thus, the target distribution is a hypothetical best-case scenario of pure growth achieved without nucleation. The closeness of matching can be expressed in a least-squares sense. By manipulation of the antisolvent and solvent flowrates in each segment (and other decision variables), we can make the fit between the model and the target distribution tighter.

Equations (3) and (6) are solved for each segment, and the output of one segment recursively becomes the input to the next segment. The procedure begins anew, with fresh antisolvent and pure solvent flowing into the main flow stream. Population density and solute concentration are adjusted for the dilution induced by addition of solvent and antisolvent at each mixing point.

4.1 Least-Squares Objective Function

The final volume fraction distribution, $f_{v,N,end}$, is used for formulating the least-squares problem:

$$\min_{\boldsymbol{d}} \sum_{i=1}^{K} (f_{v,N,end}^{i} - f_{v,target}^{i})^{2}$$

$$s.t.\, \text{Model equations } 3 - 13 \tag{14}$$

$$\text{constraints (discussed later)}$$

Where $\boldsymbol{d}$ is the vector of $2N + 5$ decision variables, and $f_{v,N,end}$ is the volume fraction size distribution at the exit of the crystallizer. It is computed as:

$$f_{v,N,end} = \frac{n_{N}^{end} L^{3}}{\int_{0}^{\infty} n_{N}^{end} L^{3}\, dL} \tag{15}$$

The index i in (14) refers to a particular crystal size bin, with K total bins. Note that n integrates to n_{total} (the total number of crystals in the solution), while $f_{v,N,end}$ integrates to 1. We use the volume fraction distribution instead of the number density, since the addition of extra solvent and antisolvent causes dilution.

4.2 List of Decision Variables and Bound Constraints

All $2N + 5$ decision variables in these optimizations had bound constraints. Table 3 below summarizes the decision variables and their lower/upper bounds.

Table 3. Decision variables and bound constraints for in-situ fines dissolution optimization.

Decision Variable	Title	Units	Lower Bound	Upper Bound
V_{feed}	Feed flowrate of saturated solvent	[ml/min]	0	300
A_{total}	Total flowrate of antisolvent	[ml/min]	0	300
S_{total}	Total flowrate of pure solvent	[ml/min]	0	150
d_{inner}	Inner diameter of crystallizer tube	[m]	10×10^{-3}	25×10^{-3}
λ	Seed mass loading	[%]	2%	7%
$a_1, a_2, \ldots, a_N$	Antisolvent distribution fractions	[-]	0	1
$s_1, s_2, \ldots, s_N$	Pure solvent distribution fractions	[-]	0	1

The optimization of the MSMA-PFC is known to be highly non-convex, as shown by the landscape plots in Ridder et al.[17] Such problems are not amenable to gradient search, and so we have opted for a stochastic approach to circumvent the nonconvexity. The genetic algorithm (GA) is a popular tool for solving optimization problems with this kind of difficulty. To make the GA operate more smoothly, our decision variables were fractions of the total antisolvent and

total pure solvent. The flowrate into a segment j is the jth fractional distribution variable multiplied by total flow allotment.

$$A_j = a_j A_{total}$$

$$S_j = s_j S_{total}$$

(16)

4.3 Linear and Nonlinear Constraints

There were no linear inequalities in this study. The only linear constraints in this work are two equalities, which require the apportionments of total liquid flows must each sum to unity. The remaining four constraints are nonlinear inequalities. Table 4 below summarizes these constraints.

Table 4. Linear and nonlinear constraints for in-situ fines dissolution optimization.

Name	Constraint	Description	Type
c_1	$\sum_{j=1}^{N} a_i = 1$	Total fractions of added liquid flows must sum to unity.	Linear
c_2	$\sum_{j=1}^{N} s_i = 1$		
c_3	$\sigma_N^{end} - 1.05 \leq 0$	Final supersaturation is bracketed between 0.5 and 1.05.	Nonlinear
c_4	$0.5 - \sigma_N^{end} \leq 0$		
c_5	$\tau_{total} - 3600 \leq 0$	Total residence time under 3600 seconds (1 hour).	
c_6	$0.30 - Y \leq 0$	Minimum required crystal mass yield of 30%.	

In the multiple-cooling segment PFC array, residence time is constant, since flowrate of liquor into each segment is always the same. However, the addition of antisolvent and pure solvent to the liquor flow changes residence time into a nonlinear function:

$$\tau_{total} = \sum_{j=1}^{N} \tau_j = \frac{\pi d_{inner}^2 (x_{total}/N)}{4} \sum_{j=1}^{N} \frac{1}{V_{feed} + A_{total} \sum_{i=1}^{j} a_i + S_{total} \sum_{i=1}^{j} s_i} \tag{17}$$

Where x_{total}/N is the length of a single segment. The jth summand in (17) is the residence time for the jth segment, which is the segment's volume divided by the total flow rate through that segment. The total residence time is found by summing over all j individual residence times. Since each PFC segment's volume is the same, it is taken out of the summation distributively.

Yield is calculated in the following manner:

$$Y = \frac{V_{feed}\rho_{H_2O}C_0 - (V_{feed}\rho_{H_2O} + S_{total}\rho_{H_2O} + A_{total}\rho_{EtOH})C_N^{end}}{V_{feed}\rho_{H_2O}C_0} \tag{18}$$

If $C_N^{end} = 0$, then all of the solute has been crystallized, and thus $Y = 1$. If no crystallization has occurred, the numerator will be zero, and thus $Y = 0$. If seed crystals have been dissolved due to excessive dissolution, then Y can become negative.

5. Solution of Least-Squares Problem by the Genetic Algorithm

5.1 Nonconvexity of Search Space

The genetic algorithm is an optimization algorithm based on the theory of natural selection. Briefly, solutions to the optimization problem are filtered by starting with a large initial "population", and judging their "fitness" in terms of the score they output when substituted into the objective function. "Unfit" candidates are eliminated from the gene pool, while the survivors have "children" with each other by various genetic operators of crossover and mutation. This

process repeats itself for several "generations" or until a certain tolerance threshold on the objective function is satisfied. More complexity arises when constraints are introduced into the problem. The GA is less efficient compared to gradient-based methods, such as sequential quadratic programming (SQP). However, algorithms like SQP are not robust to initial guess, and can become trapped in a sub-optimal local minimum.[22,23] This is true when the objective function and/or constraints are non-convex. Stochastic methods, such as the GA or simulated annealing, are appropriate for nonconvex optimization.

5.2   Genetic Algorithm Solution

The problem was solved by manipulating the $2N + 5$ decision variables with the genetic algorithm (GA). The initial population was created by randomly sampling over the bounds given in Table 3. The number of injections was arrived at through trial and error. The number of injections could not be used as a decision variable, as MATLAB's current genetic algorithm cannot solve mixed-integer nonlinear programming (MINLP) problems that have any type of equality constraint. The number of injections used was 50, which gave a good tradeoff between curve fit and computation time. The population size was 750, repeated for up to 25 generations. The MATLAB integrator, depending on the particular run, was chosen for the quickest solution time. Either ode45, ode15s, or ode23 were used.

6.   Results and Discussion

To investigate the crystallizer's performance for various kinetic parameters and total lengths, a reduced orthogonal array experimental design was used, with five factors, four levels, and 16 total runs. The five factors are the nucleation and growth parameters, and the total crystallizer length. The five factors and the four levels used are shown in Table 5 below.

Table 5. Table of the five factors and four levels used for examining parameter space.

Level	Nucleation rate constant, k_b [#/m²·s]	Nucleation order, b [-]	Growth rate constant k_g [µm/s]	Growth order g [-]	Total length of crystallizer, x_{total} [m]
1	1×10^6	1	0.1	1	5
2	1×10^7	2	0.5	1.333	10
3	1×10^8	3	1	1.667	15
4	1×10^9	4	5	2	20

A reduced design was used, since exhaustive search over $4^5 = 1024$ different optimizations was computationally prohibitive. This experimental table is given in Table 6. The orthogonal array table allows for a good sampling of the parameter space with only 16 samples instead of 1024.

Table 6. Experimental design table of factors and levels for the curve fit optimizations conducted. The numbers correspond to the level column in Table 5. The sum of the squares of the errors (SSE) and total amount of pure solvent added (S_{total}) are given for each run.

Run #	k_b	b	k_g	g	x_{total}	SSE	S_{total}
1	1	1	1	1	1	2.67E+07	80
2	1	2	2	2	2	4.71E+06	0
3	1	3	3	3	3	1.25E+07	1
4	1	4	4	4	4	7.58E+05	1
5	2	1	2	3	4	5.62E+08	3
6	2	2	1	4	3	7.42E+08	0
7	2	3	4	1	2	2.25E+07	2

8	2	4	3	2	1	6.93E+07	0
9	3	1	3	4	2	2.22E+09	8
10	3	2	4	3	1	2.10E+08	2
11	3	3	1	2	4	6.08E+09	0
12	3	4	2	1	3	3.10E+09	9
13	4	1	4	2	3	3.41E+09	11
14	4	2	3	1	4	7.82E+09	24
15	4	3	2	4	1	8.28E+09	25
16	4	4	1	3	2	1.27E+10	16

Table 6 above shows the experimental design matrix, as well as the resulting sum of the squared errors for each curve fit to the zero-nucleation target distribution.
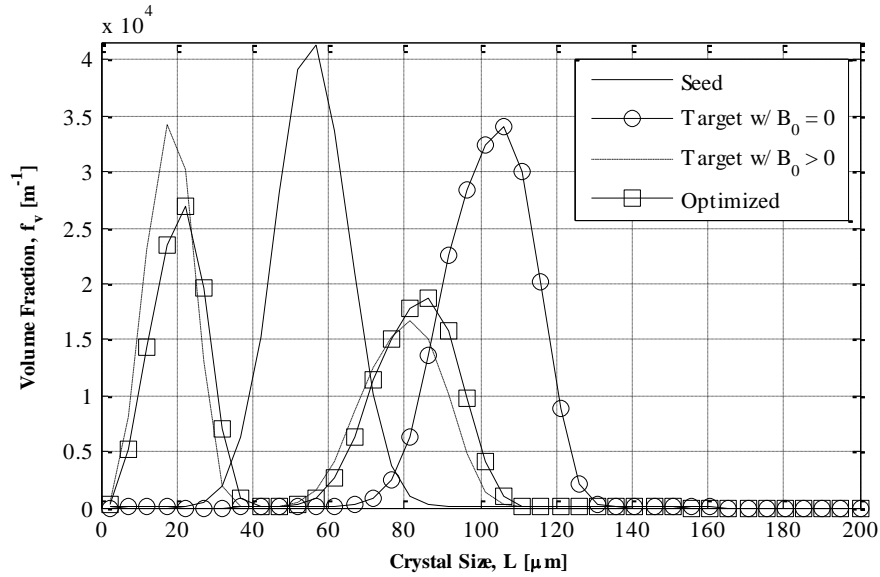
6.1 Volume Fraction Distributions for Optimized Cases

The data in Table 6 show that run #1 gave the tightest curve fit (Figure 4). The reason for this tight curve fit is due to the system exhibiting low nucleation (the k_b level is at the lowest level). Also in Figure 4. we show the performance of a single segment *with nucleation turned back on* ($B_0 > 0$). We can see there is little improvement observed between MSMA-PFC and using a single segment.
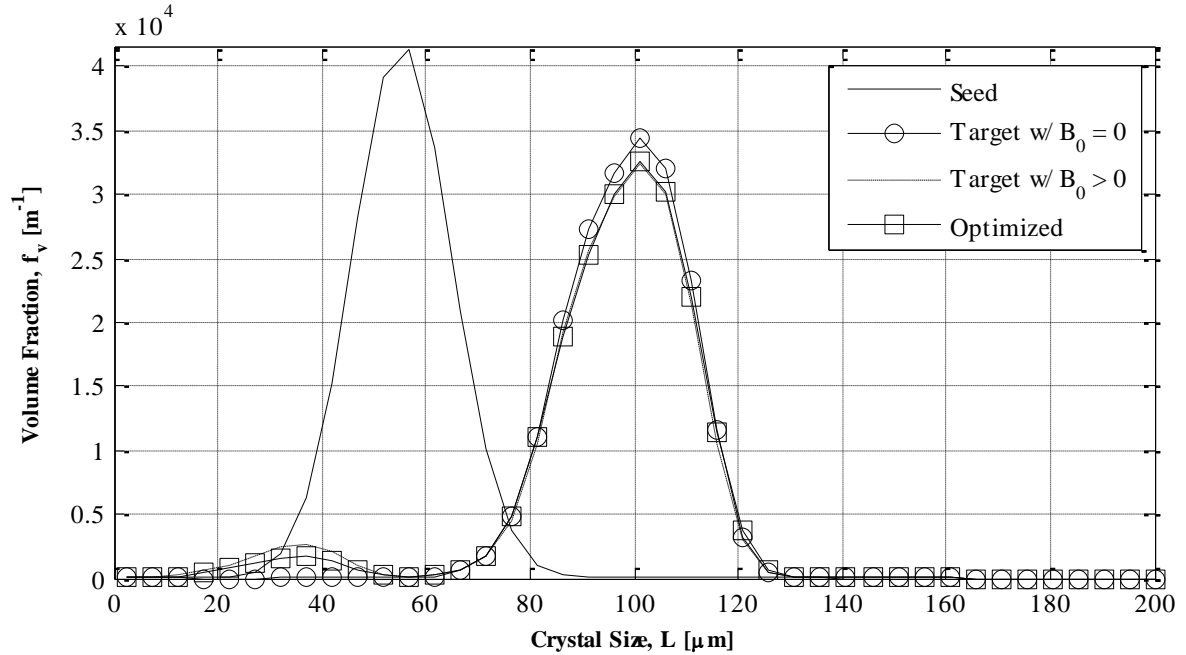
Figure 4. Volume-fraction distribution for run #1.

Increasing values of k_b rapidly degrade the curve fit due to overwhelming nucleation. Run #11 is representative of runs which are nucleation-dominated. As shown in Figure 5, there is a large amount of fines created, and the optimal result fails to hit the target distribution. While we have improved the volume fraction distribution over the single-segment case by producing less fines at the exit, there is still a great deal of fines produced. The nucleation rate constant has the greatest effect upon the performance of the crystallizer, indicating significant sensitivity to nucleation rate.

Figure 5. Volume-fraction distribution for run #11, a nucleation-dominated case.

6.2   *Main-Factor Analysis*

The results in section 6.1 suggest to us that the best results, intuitively, are obtained when the system is growth-dominated. Main-factor analysis of the experimental matrix confirms this suspicion. Main-factor analysis is done by taking the average of all SSE for a given factor *at the same level*. For example, the average for the factor k_b at level 2 would take the average SSE over runs 5, 6, 7, and 8. This process is repeated for all five factors and all four levels, which generates Table 7 below.

Table 7. Level-wise averages of SSE for each corresponding level and factor pair.

	k_b	b	k_g	g	x_{total}
L1	**1.12E+07**	**1.56E+09**	4.89E+09	2.74E+09	2.15E+09
L2	3.49E+08	2.20E+09	2.99E+09	**2.39E+09**	3.74E+09
L3	2.90E+09	3.60E+09	2.53E+09	3.38E+09	**1.82E+09**
L4	8.06E+09	3.97E+09	**9.11E+08**	2.81E+09	3.62E+09

This analysis reveals to us what the most sensitive parameters are, and also what set of levels will provide the best curve fit – which we hypothesized would be the growth-dominated case. We can see in Table 7 that the factor k_b spans the widest range of SSE values over the level averages. We thus conclude that k_b is the most sensitive parameter. Following the same line of reasoning, the second-most sensitive parameter is k_g. The optimal curve fit is projected to be the set of levels for which SSE is a minimum for each corresponding factor. These values are shown in boldface in Table 7 (they are the minimum values within each column). The main-factor analysis projects that the tightest curve fit will be observed at a k_b of level 1, a b of level 1, a k_g of level 4, a g of level 2, and an x_{total} of level 3. We term this the "projected optimum." Note that this set of factors and levels is not present in Table 6. Solving the optimization problem with this new set of parameters generates the volume fraction distributions in Figure 6, which had an SSE of 4.83×10^5, which is less than the minimum of 7.58×10^5 in Table 6.
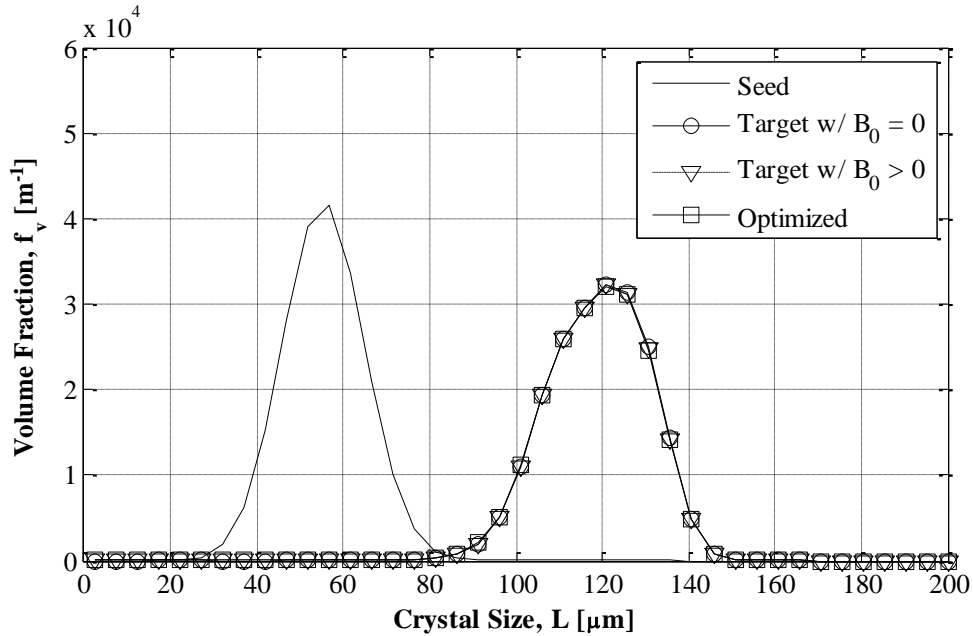
Figure 6. Optimal fit predicted by analysis of the orthogonal array design.

This result matches our intuition that the best result is obtained when nucleation is slow and growth is fast. However, this has the effect of "cancelling out" the benefits of using multiple injections, as we obtain a very tight fit to the curve anyways when using a single injection for this set of kinetic parameters. There was no discernible trend observed with respect to the optimized tube diameter. However, seed loading was typically between 5.0%-6.5%.

6.3   No Dissolution is Used to Control Fines

It is interesting (even if a bit disappointing) to observe that the optimization does not want to use dissolution to get rid of fine crystals. The total amount of pure solvent added during each optimization is given as the rightmost column in Table 6. Observe that little to no pure solvent is ever added to the system for the optimal curve fits (observe in Table 3 that S_{total} is bounded on the left by zero). The supersaturation ratio profiles (σ vs. x plots) show barely any dissolution occurring. The supersaturation profile for the "project optimum" is representative (Figure 7).
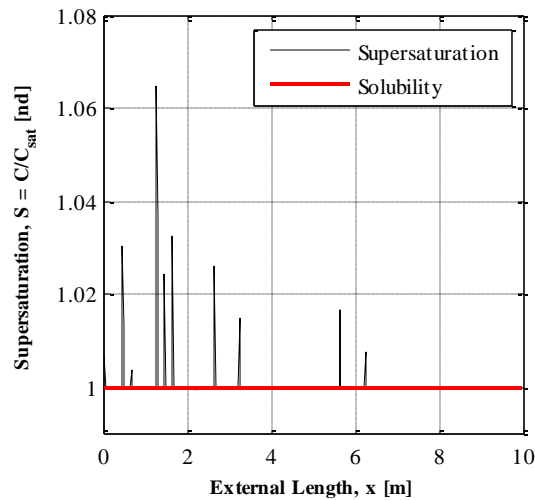
Figure 7. Supersaturation profile for project optimum, representative of the other supersaturation profiles.

Note how the supersaturation does not significantly (or at all) go below 1 anywhere in Figure 7. This indicates to us that the situations in which the curve fit is superior to the single-segment case (Figure 4 and Figure 5) is more likely due to the better control offered by using multiple segments (and thus having finer control over supersaturation), rather than making use of fines dissolution. The reason the optimization refuses to add pure solvent in significant amounts is due to the fact that adding pure solvent reduces the concentration (via dilution) and reduces available residence time (via equation (17)). Reduced concentration reduces the available supersaturation, and reducing the residence time reduces the time available for growth inside the MSMA-PFC. Thus, despite the potential for dissolving fines, the benefit of adding pure solvent does not counterbalance the other two negative phenomena.

7. Summary and Conclusions

We have investigated the optimal operation of antisolvent crystallization in a MSMA-PFC and explored the feasibility of dissolution steps by addition of pure solvent in order to dissolve the fine crystals in-situ. The model equations solved were the population balance equation and the

integro-differential mass balance equation. The solution method used was the finite volume method, since the entire CSD was required to calculate the sum of the squared errors for the curve fit. The final CSD was compared to a target CSD generated by arbitrarily setting nucleation to zero. A reduced orthogonal array experimental design was used to examine the effect of several kinetic parameters and total crystallizer length. The genetic algorithm was used to optimize over the decision variables, with the parameters from the experimental design table held constant. The results indicate that k_b is the most sensitive parameter, followed by k_g. As k_b increases, the curve fit degrades rapidly due to becoming overwhelmed by nucleation. Examination of the supersaturation profiles shows that dissolution is not occurring appreciably for any of the optimizations performed. The MSMA-PFC performs best under kinetic crystallization conditions in which a single PFC also works sufficiently well. There are situations where using multiple additions does improve the curve fit versus the single-segment case, but excessive fines still exist. The reason the optimization does not add any pure solvent is likely due to the addition of pure solvent causing a simultaneous decrease in concentration and decrease in residence time. Both of these cause the optimization to take "one step forward and two steps back", thus adding pure solvent is judged to be sub-optimal.

To implement this system in practice, several sensors and control loops would be necessary. A variety of low-cost sensors have been developed in recent years.[24] The paper by Simon et. al. [25] reviews the state of the art with regards to sensors, but only a few are feasible for use in this system. Ultrasonic crystallization monitoring (UCM) is only applicable for crystal sizes of at least 100 microns, which is too large for most of the crystals simulated in this study. Conductometry measurements for concentration are only feasible if the compound being

crystallized is inorganic. Raman spectroscopy is only necessary if a shift in polymorphic form in expected.

The most likely candidates for CSD monitoring are either/or focused beam reflectance measurement (FBRM) and video imaging, as well as FTIR for measurement of concentration. However, even these techniques may only be practical for the larger crystals, thus allowing only a portion of the crystal size distribution to be measured. FBRM signals would need to be adjusted, as FBRM only measures chord length distribution, and not crystal size distribution. The continuous nature of the crystallization suggests also a continuous approach to data collection. Data from these sensors can be viewed as a continuous stream of complex information, which requires sophisticated algorithms to process for accurate state estimation. Such methods are reviewed in Simon et. al.[25]

For feedback control, the likely measured variables would be the CSD and concentrations at the exit of the crystallizer array, which would then feedback to flow controllers for the dispensation of solvent and antisolvent. Adjustment of flow rates to the individual segments would function as feedback actuation method. Comparison between the expected CSD and measured CSD, and expected concentration and measured concentration, would drive the feedback control. A more complicated approach would be to have CSD and concentration sensors in between each crystallizer segment, thus providing much more information on the evolution of the CSD as a function of length. Flow controllers could then respond much faster to process disturbances, as crystals would not need to flow all the way to the exit of the crystallizer before controller action is taken. Feedforward control also seems like a likely necessity, as the properties of the input seed crystals may not be uniform in time, and thus represent a disturbance

at the inlet of the process. Fluctuations in inlet concentration are also possible, requiring further additional control.

Some comparison with the previous work by Majumder and Nagy is in order.[16] That work is very similar to this work. In both cases, crystallization is being optimized in a least-squares sense by manipulating process parameters in order to hit a target distribution. In that work however, temperature was the method for altering supersaturation, whereas in this case we used antisolvent to alter liquid-phase composition (and hence, the supersaturation). One of the key differences between that work and this work, is that temperature cycling is observed to be the optimal strategy for the elimination of fine crystals. It was observed in that work further that the efficacy of the optimization was significantly enhanced if the crystallization and dissolution kinetics were size-dependent. We have not considered size-dependency in this work, which may be a worthwhile subject of future investigation.

Nomenclature

Symbol	Meaning	Units
$a_1, a_2, \dots, a_N$	Proportion of total antisolvent allocated to the jth segment	-
A	Antisolvent flowrate	ml/min
A_{total}	Total flowrate of added antisolvent summed over all segments	ml/min
b	Nucleation order	-
B_0	Nucleation rate	# of nucleated crystals/kg solution·s
C	Solute concentration	kg API/kg solution
C_0	Initial concentration of solute	kg API/kg solution
$C(x_j^{end})$ or C_j^{end}	Solute concentration at the end of the jth segment	kg API/kg solution
C_N^{end}	Solute concentration at the exit of the	kg API/kg solution

	crystallizer	
C_{sat}	Solubility (saturation) concentration	kg API/kg solution
d	Dissolution order	-
$\boldsymbol{d}$	Vector of decision variables	varies
d_{inner}	Inner diameter of crystallizer tube	m
D	Crystal linear dissolution rate	m/s
f_v	Volume fraction distribution	m^{-1}
$f_{v,N,end}$	Volume fraction distribution at the exit of the crystallizer	m^{-1}
$f_{v,target}$	Target volume fraction distribution	m^{-1}
g	Growth rate order	-
G	Crystal linear growth rate	μm/s or m/s
i	Dummy summation index	-
j	Index corresponding to the jth crystallizer segment	-
K	Total number of crystal size bins	-
k_b	Nucleation rate constant	# of nucleated crystals/m^2·s
k_g	Growth rate constant	m/s
k_v	Crystal shape factor, $\pi/6$	-
L	Internal coordinate; characteristic crystal length	m or μm
L_0	The smallest crystal size bin	μm
n	Number density (crystal size distribution)	# of crystals/kg of solution·m
N	Number of crystallizer segments	-
n_0	Seed crystal size distribution	# of crystals/kg of solution·m
$n\left(L,x_j^{end}\right)$ or n_j^{end}	Number density at the end of the jth segment	# of crystals/kg of solution·m
n_N^{end}	Crystal size distribution at the exit of the crystallizer	# of crystals/kg of solution·m
N_{total}	Total number density of crystals	# of crystals/kg solution
S	Pure solvent flowrate	ml/min
$s_1, s_2, \dots, s_N$	Proportion of total pure solvent allocated to the jth segment	-
S_{total}	Total flowrate of added pure solvent, summed over all segments	ml/min

SSE	Sum of the squared errors	varies
u_x	Average velocity in the x-direction	m/s
V_{feed}	Saturated mother liquor at flowrate	ml/min
$V^{solution}$	Volumetric flowrate of entire solution stream, containing both solvent and antisolvent	ml/min
x	External coordinate; distance along a crystallizer segment	m
X_{H_2O}	Mass fraction of water	-
x_{total}	Total length of the entire crystallizer	m
Y	Crystal mass yield	-
Greek Symbols		
γ	Dilution correction factor	-
$\delta(L - L_0)$	Dirac delta function, with pulse centered at L_0	m^{-1}
δ_{seed}	Mean of seed distribution Gaussian bell curve	m
λ	Seed mass loading	%
μ_k	k^{th}-moment of the crystal size distribution	m^k/kg solution
ρ_c	Density of solid API crystals	kg/m^3
ρ_{EtOH}	Density of ethanol	kg/m^3
ρ_{H_2O}	Density of water	kg/m^3
$\rho^{solution}$	Density of solution	kg/m^3
σ	Supersaturation ratio	-
τ_j	Residence time in the jth segment	s
τ_{total}	Total residence time of the crystallizer array	s
φ	Dissolution acceleration	-
ω_{seed}	Standard deviation of seed distribution Gaussian bell curve	m

References

(1) Schaber, S. D.; Gerogiorgis, D. I.; Ramachandran, R.; Evans, J. M. B.; Barton, P. I.; Trout, B. L. Economic Analysis of Integrated Continuous and Batch Pharmaceutical Manufacturing: A Case Study. *Ind. Eng. Chem. Res.* **2011**, *50* (17), 10083.

(2)   Alvarez, A. J.; Myerson, A. S. Continuous Plug Flow Crystallization of Pharmaceutical Compounds. *Cryst. Growth Des.* **2010**, *10* (5), 2219.

(3)   Nagy, Z. K.; Fevotte, G.; Kramer, H.; Simon, L. L. Recent Advances in the Monitoring, Modelling and Control of Crystallization Systems. *Chem. Eng. Res. Des.* **2013**, *91* (10), 1903.

(4)   Abel, M. J. Process Systems Engineering of Continuous Pharmaceutical Manufacturing. Dissertation, MIT: Cambridge, MA, 2010.

(5)   Benyahia, B.; Lakerveld, R.; Barton, P. I. A Plant-Wide Dynamic Model of a Continuous Pharmaceutical Process. *Ind. Eng. Chem. Res.* **2012**, *51* (47), 15393.

(6)   Vervaet, C.; Remon, J. P. Continuous Granulation in the Pharmaceutical Industry. *Granulation Length Scales - 2nd Int. Workshop Granulation Granulation Length Scales - 2nd Int. Workshop Granulation* **2005**, *60* (14), 3949.

(7)   Vehring, R. Pharmaceutical Particle Engineering via Spray Drying. *Pharm. Res.* **2008**, *25* (5), 999.

(8)   Roche, F.; Page, T.; Seville, J. Non-Stop Pharma. *TCE - The Chemical Engineer*. February 2013, pp 28–31.

(9)   Mollan Jr., M. J.; Lodaya, M. Continuous Processing in Pharmaceutical Manufacturing. *Pharmaceutical Manufacturing Magazine*. 2004.

(10)   Reutzel-Edens, S. M. Achieving Polymorph Selectivity in the Crystallization of Pharmaceutical Solids: Basic Considerations and Recent Advances. *Curr. Opin. Drug Discov. Devel.* **2006**, *9* (6), 806.

(11)   Jones, A. G. *Crystallization Process Systems*; Butterworth-Heinemann: Oxford, 2002.

(12)   Tavare, N. S. *Industrial Crystallization: Process Simulation, Analysis, and Design*; Plenum Chemical Engineering Series; Plenum: New York, 1995.

(13)   Abu Bakar, M. R.; Nagy, Z. K.; Saleemi, A. N.; Rielly, C. D. The Impact of Direct Nucleation Control on Crystal Size Distribution in Pharmaceutical Crystallization Processes. *Cryst. Growth Des.* **2009**, *9* (3), 1378.

(14)   Rodríguez-hornedo, N.; Murphy, D. Significance of Controlling Crystallization Mechanisms and Kinetics in Pharmaceutical Systems. *J. Pharm. Sci.* **1999**, *88* (7), 651.

(15)   Sen, M.; Chaudhury, A.; Singh, R.; John, J.; Ramachandran, R. Multi-Scale Flowsheet Simulation of an Integrated Continuous Purification–downstream Pharmaceutical Manufacturing Process. *Int. J. Pharm.* **2013**, *445* (1–2), 29.

(16)   Majumder, A.; Nagy, Z. K. Fines Removal in a Continuous Plug Flow Crystallizer by Optimal Spatial Temperature Profiles with Controlled Dissolution. *AIChE J.* **2013**, *59* (12), 4582.

(17)   Ridder, B. J.; Majumder, A.; Nagy, Z. K. Population Balance Model-Based Multiobjective Optimization of a Multisegment Multiaddition (MSMA) Continuous Plug-Flow Antisolvent Crystallizer. *Ind. Eng. Chem. Res.* **2014**, *53* (11), 4387.

(18)   Ridder, B. J.; Majumder, A.; Nagy, Z. K. Population Balance Model Based Multi-Objective Optimization and Robustness Analysis of a Continuous Plug Flow Antisolvent Crystallizer. *Am. Control Conf. ACC 2014* **2014**, 3530.

(19)   Luo, Y.-H.; Wu, G.-G.; Sun, B.-W. Antisolvent Crystallization of Biapenem: Estimation of Growth and Nucleation Kinetics. *J. Chem. Eng. Data* **2013**, *58* (3), 588.

(20)   Randolph, A. D.; Larson, M. A. *Theory of Particulate Processes: Analysis and Techniques of Continuous Crystallization*; Academic Press: New York, 1971.

(21)   Gunawan, R.; Fusman, I.; Braatz, R. D. High Resolution Algorithms for Multidimensional Population Balance Equations. *AIChE J.* **2004**, *50* (11), 2738.

(22)   Beers, K. J. *Numerical Methods for Chemical Engineering: Applications in Matlab*; Cambridge University Press, 2006.

(23)   Press, W. H.; Teukolsky, S. A.; Vetterling, W.; Flannery, B. P. *Numerical Recipes in C - The Art of Scientific Computing*, 2nd ed.; Cambridge University Press: New York, 1992.

(24)   Simon, L. L.; Merz, T.; Dubuis, S.; Lieb, A.; Hungerbuhler, K. In-Situ Monitoring of Pharmaceutical and Specialty Chemicals Crystallization Processes Using Endoscopy–stroboscopy and Multivariate Image Analysis. *Chem. Eng. Res. Des. 90* (11), 1847.

(25)   Simon, L. L.; Pataki, H.; Marosi, G.; Meemken, F.; Hungerbühler, K.; Baiker, A.; Tummala, S.; Glennon, B.; Kuentz, M.; Steele, G.; et al. Assessment of Recent Process Analytical Technology (PAT) Trends: A Multiauthor Review. *Org. Process Res. Dev.* **2015**, *19* (1), 3.

For Table of Contents Only